Junior Sophomore Experimental Physics Laboratory Report

Trinity College Dublin, School of Physics

Laboratory 1: The Zeeman Effect

Matthew Dunne

October 9, 2023

1 Abstract

In this experiment, we investigated the changing properties of the red spectrum of neutral Cadmium gas in the presence of a magnetic field. The setup included a Fabry Perot etalon which created a ring shaped interference pattern by causing single beams of light to split and then interfere. The interference pattern was used to determine the wavelength of the red Cadmium line which was found to be $\lambda = 639 \pm (20) nm$. When an external magnetic field was introduced, it was observed that the lines in the spectrum could split into doublets or triplets depending on the field's orientation and this is the Zeeman effect. We compared the longitudinal and transverse normal Zeeman effect by finding the polarisation states of the lines in the interference pattern and determining the shift in the wavelength ($\Delta\lambda$) for varying field strengths corresponding to different values of current in the electromagnet. In particular, it was found that this shift only depended on the strength but not the direction of the magnetic field. Contrarily, the polarisation states of the doublet and triplet lines depended mainly on the direction of the field. A value was obtained for the Bohr magneton $\mu_B = 8.024 \times 10^{-24} \pm 0.5 \times 10^{-24}$ which varies from the value found in literature by approximately 15%, although this could be explained by systematic experimental error

2 Introduction and Theory

The Zeeman effect, first discovered by Peter Zeeman in 1896[1], is a phenomenon in which the electron energy levels of an atom are shifted in the presence of an external

magnetic field. When it was first discovered, it was not understood theoretically since the theory of quantum mechanics had not yet been formulated. Fortunately, in modern times it is well understood and can be explained as follows. Consider a single electron under the influence of an external magnetic field B, which is weak in comparison to the internal magnetic field of the electron (or more generally the atom to which the electron is attributed). Its Hamiltonian will be perturbed by a factor

$$H'_{Zeeman} = -(\vec{\mu_l} + \vec{\mu_s}) \cdot \vec{B}, \tag{2.1}$$

where $\vec{\mu_s}$ is the magnetic dipole moment due to electron spin and $\vec{\mu_l}$ is the magnetic dipole moment associated with orbital angular momentum. Respectively, the dipole moments are defined as

$$\mu_s = -\frac{e}{m}\vec{S}, \qquad \mu_l = -\frac{e}{2m}\vec{L}, \tag{2.2}$$

then the perturbation can be written as

$$H'_{Zeeman} = \frac{e}{2m}(\vec{L} + 2\vec{S}) \cdot \vec{B} \tag{2.3}$$

The shift in the electron energy caused by this perturbation is then given by

$$\Delta E_{Zeeman} = \frac{e}{2m}\vec{B} \cdot \langle \vec{L} + 2\vec{S} \rangle, \tag{2.4}$$

the total angular momentum vector $\vec{J} = \vec{L} + \vec{S}$ is a constant vector around which $\vec{L}$ and $\vec{S}$ precess and we can write $\vec{L} + 2\vec{S} = \vec{J} + \vec{S}$. Then the average of the spin vector is just its projection along the total angular momentum vector

$$\vec{S}_{average} = \frac{\vec{S} \cdot \vec{J}}{J^2}\vec{J} \tag{2.5}$$

we can extract the dot product of $\vec{S}$ and $\vec{J}$ from $L^2 = J^2 + S^2 - 2\vec{S} \cdot \vec{J}$, thus

$$\langle \vec{L} + 2\vec{S} \rangle = \left\langle 1 + \left(\frac{\vec{S} \cdot \vec{J}}{J^2} \right) \vec{J} \right\rangle = \left[1 + \frac{J(J+1) + S(S+1) - L(L+1)}{2J(J+1)} \right] \langle \vec{J} \rangle. \tag{2.6}$$

The term within square brackets is called the Landé g-factor g_J. Then letting the z-direction be defined by $\vec{B}$, we have that $\langle \vec{J} \rangle = M_J$ which is the z-component of J with $(2J+1)$ eigenvalues. Finally, the total shift in the energy of the electron is[2]

$$\Delta E_{Zeeman} = \mu_B g_J B M_J, \tag{2.7}$$

where $\mu_B = e\hbar/2m = 5.7788 \times 10^{-5}\ eV/T = 9.274 \times 10^{-24} J/T$ is the Bohr magneton. This formula tells us that each level corresponding to an eigenvalue of M_J has the same energy when $B = 0$ but the introduction of the field splits these degenerate energy levels into independent levels.

In this experiment, we will observe the *normal* Zeeman effect as the splitting of spectral lines corresponding to atomic energy levels in neutral cadmium. In this case, the word "normal" is reserved for splitting of spectral lines resulting from transitions between two $S = 0$ states. The other case is the *anomalous* Zeeman effect as discovered by Thomas Preston of Trinity College Dublin in 1898[3] where both states have a non-zero spin quantum number.

We are able to predict the spectrum we expect to see in both the transverse and longitudinal Zeeman effect by considering the selection rules for electric dipole transitions. The photon has spin-1, meaning that $\Delta M_J = (0, \pm 1)$ correspond to the transitions which are allowed. Since we let the magnetic field define the z-direction, transverse viewing is done perpendicular to the field, whereas longitudinal viewing is done along the z-direction. $\Delta M_J = 0$ transitions result in dipole oscillations along the z-axis meaning that the photons from this transition are not visible longitudinally! $\Delta M_J = \pm 1$ transitions correspond to left and right hand rotating dipole oscillations in the x-y plane. The resulting circularly polarised radiation will be emitted in the z-direction. When viewed in the transverse configuration, the circular oscillations will appear as plane-polarised light. This means that for the transverse normal Zeeman effect, we should expect to see a line triplet and a line doublet in the longitudinal configuration. We can derive the wavelength of each line in as follows

$$\frac{\Delta\lambda}{\lambda_0} = \frac{\Delta E}{E} \implies \Delta\lambda = \frac{\lambda_0^2 \mu_B B \Delta M_J}{hc}, \tag{2.8}$$

where we have used equation (2.7). Then by substituting in our three available values for ΔM_J we find that the wavelengths of each line in the triplet for the transverse effect are $\lambda = \lambda_0,\ \lambda_0 \pm \lambda_0^2 \mu_B B/hc$. For the longitudinal effect the $\Delta M_J = 0$ transition is not visible thus the wavelengths of the doublet lines will be $\lambda_0 \pm \lambda_0^2 \mu_B B/hc$.

3 Experimental Setup

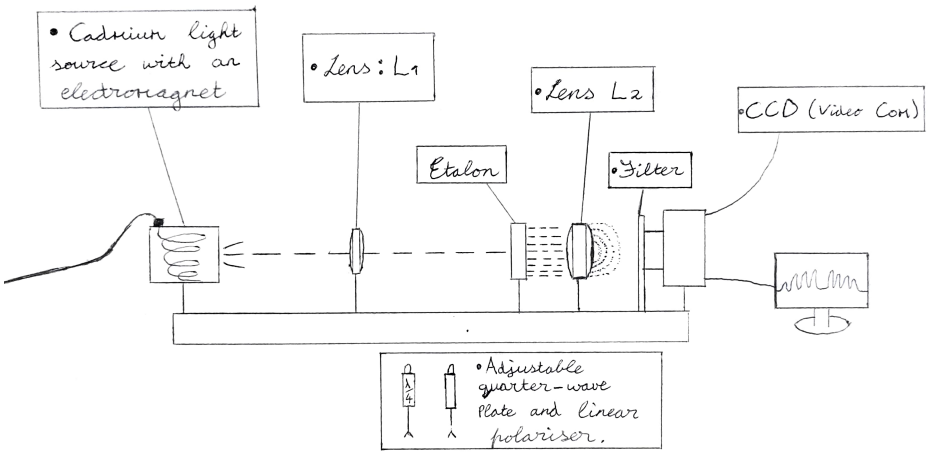

Figure 3.1: A sketch of the equipment used to conduct experiments on the Zeeman effect in the spectrum of neutral Cadmium.

The filter used restricts the observed light to the red band of the optical spectrum, the anomalous Zeeman effect can also be found in the blue spectrum of Cadmium therefore its is important for the filter to isolate the results of the normal Zeeman effect. The CCD (2048 pixel) array camera monitors intensity across a thin horizontal slice of the incoming pattern of light. Note that each pixel corresponds to a length of $14\mu m$. The etalon has a thickness ($d = 4.00mm$) and refractive index ($n = 1.457$), it is used to split an incident beam into multiple beams by virtue of its highly reflective surfaces. The first lens L_1 focuses the incident light onto the etalon and the second L_2 (focal length $f = 150mm$) focuses the interference pattern of multiple beams produced by the etalon onto the CCD. The setup also includes a quarter wave plate and a linear polariser which can be used to verify the previous discussion about the polarisation states.

The pattern generated by this setup is a series of ordered fringes in the form of concentric rings, to show why this is the case one must consider the operation of the etalon. When a ray of light enters the etalon at an angle β with respect to the optical axis, it is reflected from each wall within the etalon multiple times with a small amount of the light escaping upon each reflection. The path difference between successive rays exiting the etalon at an angle α relative to the optical axis is

$$\Delta = 2d\sqrt{n^2 - \sin^2\alpha} = 2nd\sqrt{1 - \sin^2\beta} = 2nd\cos\beta \tag{3.1}$$

In a similar fashion to the phenomenon of thin-film interference, the rays emerging from the etalon at an angle α_m only constructively interfere when their path difference is equal

to an integer multiple of the wavelength. Furthermore, when a ring of radius r is viewed in the focal plane of L_2 we have a right triangle for which $\tan(\alpha) = r/f$. Combining these two facts we have that for small angles α

$$m\lambda = 2nd\sqrt{1 - \frac{\sin^2\alpha}{n^2}} \approx 2nd\sqrt{1 - \frac{\tan^2\alpha}{n^2}} \approx 2nd\left(1 - \frac{r_m^2}{2n^2f^2}\right), \tag{3.2}$$

where we have used that the Taylor expansion of $\sqrt{1-x^2}$ for small x is $1 - x^2/2$. Note that r_m denotes the radius of the ring of order m in the interference pattern. Then we can derive one last vital expression for the experiment which describes how a shift in the wavelength $\Delta\lambda$ affects the radius of the m'th ring r_m

$$\frac{\lambda + \Delta\lambda}{\lambda} = \frac{1 - \frac{(r+\Delta r)^2}{2n^2f^2}}{1 - \frac{r^2}{2n^2f^2}} \implies \frac{\Delta\lambda}{\lambda} \approx 1 - \frac{2r\Delta r}{2n^2f^2} - 1 + \mathcal{O}(r^2, \Delta r^2) \implies \frac{\Delta\lambda}{\lambda} = \frac{r\Delta r}{n^2f^2}. \tag{3.3}$$

4 Methodology

1: Determination of Wavelength

First, the Cadmium lamp was switched on and it was noted that a fuzzy circle of light could be observed through the eyepiece. In order to produce a sharp and bright circular interference pattern, the L_1 lens was adjusted from the light source towards the etalon slowly until the position allowing for maximum intensity was found. The L_2 lens and etalon were then adjusted slightly so that the eyepiece was in the focal plane of the lens and the lens was an appropriate distance from the etalon allowing the projection of its signature ring pattern at the highest possible resolution. The eyepiece was then replaced with the CCD camera and the radius of the first ten interference peaks on both sides of the distribution were recorded, the average of both sides was then used in calculations. The wavelength could then be found using equation (3.2) which suggests that the slope of the graph m versus r_m^2 is $(\lambda_0 nf^2/d)$

2: Transverse Normal Zeeman Effect

The equipment was once again set up using the eyepiece which was replaced by the CCD. The electromagnet was then used in the transverse orientation to generate a magnetic field by increasing the current (I) through the coil. As the current was increased, it was recorded that each line in the interference pattern began to split into a triplet. The radius (r_m) was recorded for as many peaks as possible (up to $m = 6$) along with the distance by which the peaks had shifted in the line triplets (Δr) for $I = (4, 5, 6, 7)A$. This was done on both the left and right side of the distribution so that the average could be taken to reduce any potential error caused by a-symmetry. The results were tabulated as the average of the results from each side of the distribution. A graph of the mean of $r\Delta r$ against $|\vec{B}|$ for each current was produced. Equation (3.3) was used to find

the shift $\Delta\lambda$ for each value of $|\vec{B}|$ and these values for the shift were used in equation (2.8) to find the value of the Bohr magneton. The polarisation states were determined using the quarter-wave plate and linear polariser at $I = 7A$.

3: Longitudinal Normal Zeeman Effect

The equipment was set up exactly as in the previous section and then the electromagnet was rotated by 90 deg so that the magnetic field was oriented along the optical axis. An identical set of steps to section (2) was then carried out with the exception of graphing the already established relationship between $\Delta\lambda$ and $|\vec{B}|$.

5 Results and Discussion

1: Determination of Wavelength

After tuning the setup to produce the optimal interference pattern at the highest possible sharpness, the image in Figure (5.1) shown below could be seen through the eyepiece.

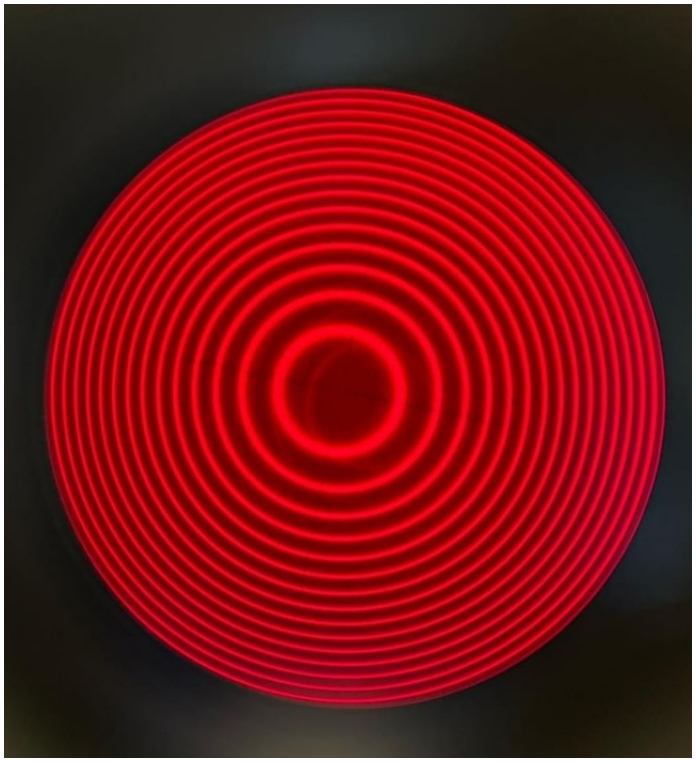

Figure 5.1: Concentric Ring interference pattern caused by the beam splitting effect in the etalon resolved by lens L_2.

The results of measuring the radius of the first ten peaks on the left and right side of the distribution and taking the average were:

Radius Measurements for Section 1 using CCD			
Order: m	r_m (pixels)	r_m^2 (m^2)	δr_m^2 (m^2)
1	112.3	2.47×10^{-6}	4.12×10^{-8}
2	199.1	7.77×10^{-6}	1.16×10^{-8}
3	257.1	1.30×10^{-5}	7.06×10^{-9}
4	304.4	1.82×10^{-5}	5.72×10^{-9}
5	345.1	2.33×10^{-5}	5.20×10^{-9}
6	382.1	2.86×10^{-5}	4.71×10^{-9}
7	415.6	3.39×10^{-5}	3.88×10^{-9}
8	446.9	3.91×10^{-5}	3.97×10^{-9}
9	476.0	4.44×10^{-5}	2.90×10^{-9}
10	503.7	4.97×10^{-5}	2.68×10^{-9}

Plotting r_m^2 against m for the first ten peaks acquired the graph shown in Figure (5.2)

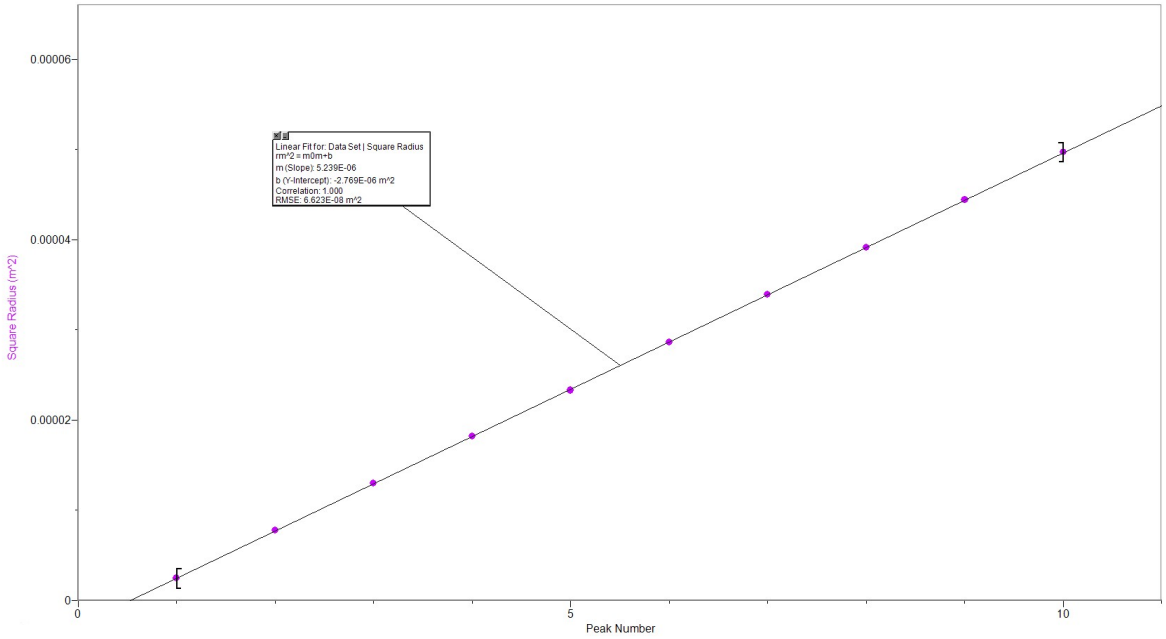

Figure 5.2: A plot of the radius-squared against peak number for $m = 1, \ldots, 10$ with a linear fit used to determine the slope. Note the error bars were included here but were small enough to not appear through the original data points.

Using the analysis tools of the Logger Pro software it was determined that the slope was $M = 5.293 \times 10^-6 \pm 7 \times 10^{-8}(m^2)$. Using equation (3.2), it was determined that $\lambda_0 = 6.39 \times 10^{-7} \pm 2 \times 10^{-8}$. Where the error was calculated using the standard propagation of uncertainty formula. The obtained value $\lambda_0 = 639 \pm 20nm$ is comparable to the accepted value in literature of $643.84nm$ within experimental error.

Transverse Normal Zeeman Effect

When using the current through the electromagnet to generate a magnetic field, the following table of values from the lab manual[4] was used to find values of $|\vec{B}|$

I [increasing] (A)	B (mT)	I [decreasing] (A)	B (mT)
4	394	7	594
5	485	6	555
6	552	5	493
7	594	4	407

The table displays different values of B for identical values of current depending on whether the current was increased or decreased to a given value. This is because the induction of a magnetic field by a current has an associated *lagging effect* commonly referred to as a hysteresis loop.

After turning the current slowly to $I = 7A$ the image seen through the eyepiece appeared as seen in Figure (5.3) below:

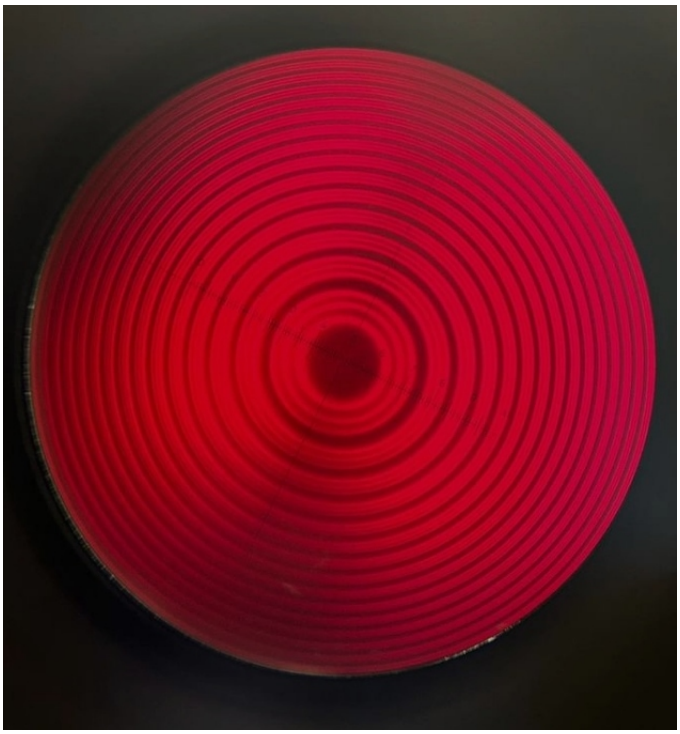

Figure 5.3: Concentric ring interference pattern viewed in the transverse orientation of a magnetic field.

It is clear to see that the atomic degeneracy had been lifted by the magnetic field as we see line triplets instead of individual lines for each ring. All three of the (now independent) electron energy transitions occur with equal probability which is why the triplet

was faint in comparison to the singlet lines seen in Figure (5.1) above.

After measuring the radius r_m and the radius shift of each outer triplet component Δr for a range of I the results were tabulated as shown below: (note that the error associated with a measurement in pixels is ± 1 pixel which translates to $\pm 14\mu m$)

Peak Radii and Shift of Radii for $I = 4A$					
m	r_m (pixels)	r_m (m)	Δr_m (m)	$r_m \Delta r_m$ (m^2)	$\delta r_m \Delta r_m$ (m^2)
1	118.9	1.66×10^{-3}	2.19×10^{-4}	3.64×10^{-7}	3×10^{-8}
2	204.2	2.86×10^{-3}	1.29×10^{-4}	3.69×10^{-7}	4×10^{-8}

The triplets for $m > 2$ were not resolved enough to measure, then:

Peak Radii and Shift of Radii for $I = 5A$					
m	r_m (pixels)	r_m (m)	Δr_m (m)	$r_m \Delta r_m$ (m^2)	$\delta r_m \Delta r_m$ (m^2)
1	120.1	1.68×10^{-3}	2.88×10^{-4}	4.84×10^{-7}	3×10^{-8}
2	204.8	2.87×10^{-3}	1.63×10^{-4}	4.68×10^{-7}	4×10^{-8}
3	263.7	3.69×10^{-3}	1.27×10^{-4}	4.69×10^{-7}	5×10^{-8}

In this case, the triplets of order $m > 3$ were not resolved enough to measure, then:

Peak Radii and Shift of Radii for $I = 6A$					
m	r_m (pixels)	r_m (m)	Δr_m (m)	$r_m \Delta r_m$ (m^2)	$\delta r_m \Delta r_m$ (m^2)
1	121.2	1.70×10^{-3}	3.39×10^{-4}	5.76×10^{-7}	3×10^{-8}
2	205.5	2.88×10^{-3}	1.94×10^{-4}	5.59×10^{-7}	4×10^{-8}
3	264.0	3.70×10^{-3}	1.49×10^{-4}	5.50×10^{-7}	5×10^{-8}
4	311.7	4.36×10^{-3}	1.26×10^{-4}	5.49×10^{-7}	6×10^{-8}
5	353.1	4.94×10^{-3}	1.11×10^{-4}	5.46×10^{-7}	7×10^{-8}
6	390.2	5.46×10^{-3}	9.45×10^{-5}	5.16×10^{-7}	8×10^{-8}

With the last set of results being:

Peak Radii and Shift of Radii for $I = 7A$					
m	r_m (pixels)	r_m (m)	Δr_m (m)	$r_m \Delta r_m$ (m^2)	$\delta r_m \Delta r_m$ (m^2)
1	122.7	1.71×10^{-3}	3.73×10^{-4}	6.39×10^{-7}	3×10^{-8}
2	206.3	2.89×10^{-3}	2.14×10^{-4}	6.19×10^{-7}	4×10^{-8}
3	264.7	3.71×10^{-3}	1.77×10^{-4}	6.56×10^{-7}	5×10^{-8}
4	312.3	4.37×10^{-3}	1.40×10^{-4}	6.12×10^{-7}	6×10^{-8}
5	353.6	4.95×10^{-3}	1.20×10^{-4}	5.93×10^{-7}	7×10^{-8}
6	390.5	5.47×10^{-3}	1.08×10^{-4}	5.90×10^{-7}	8×10^{-8}

In equation (3.3) we see that $r\Delta r$ should be the same for each triplet, this is because the expression does not depend on the order m. From the tables above we see that this holds quite strongly for the values of $r\Delta r$ calculated in the lab. Taking the average of these for each value of I we can plot how $r\Delta r$ is related to the magnetic field strength B, the resulting graph is shown below in Figure (5.4).

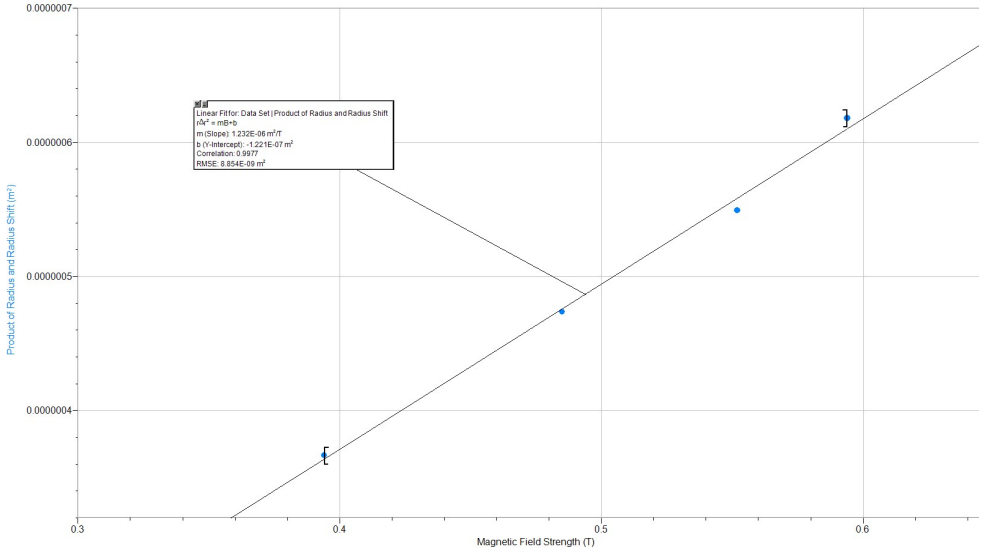

Figure 5.4: A plot of the mean value of $r\Delta r$ versus the magnetic field strength B in the transverse normal Zeeman effect for multiple values of I.

Analysing the data of the above figure under a linear regime returns a strong-positive correlation with correlation coefficient $r = 0.9977$. This shows that indeed $r\Delta r \propto B$, combined with equation (3.3) we see that this implies $\Delta\lambda \propto B$ and we can calculate the Bohr magneton μ_B by substituting in equation (2.8) which reveals that

$$r\Delta r = \left(\frac{n^2 f^2 \mu_B \lambda_0}{hc}\right) B. \tag{5.1}$$

Thus setting the slope of the graph equal to the term in brackets we obtain $\mu_B = 8.024 \times 10^{-24} \pm 0.5 \times 10^{-24}$. This value is only correct up to ($\approx 15\%$) of the accepted value 9.274×10^{-24}. Unfortunately this is quite a high percentage error and we believe it was caused by the lack of measurements we were able to make for the smaller magnetic field strengths. In particular, for the points on the graph corresponding to $I = (4, 5)A$ it is safe to say that they fail to represent the true value of $r\Delta r$ having only been calculated for two or three interference maxima.

After adding the quarter wave plate and the linear polariser, observations showed that the polarisation states of the triplet lines could be seen most prominently in the following two graphs of intensity:

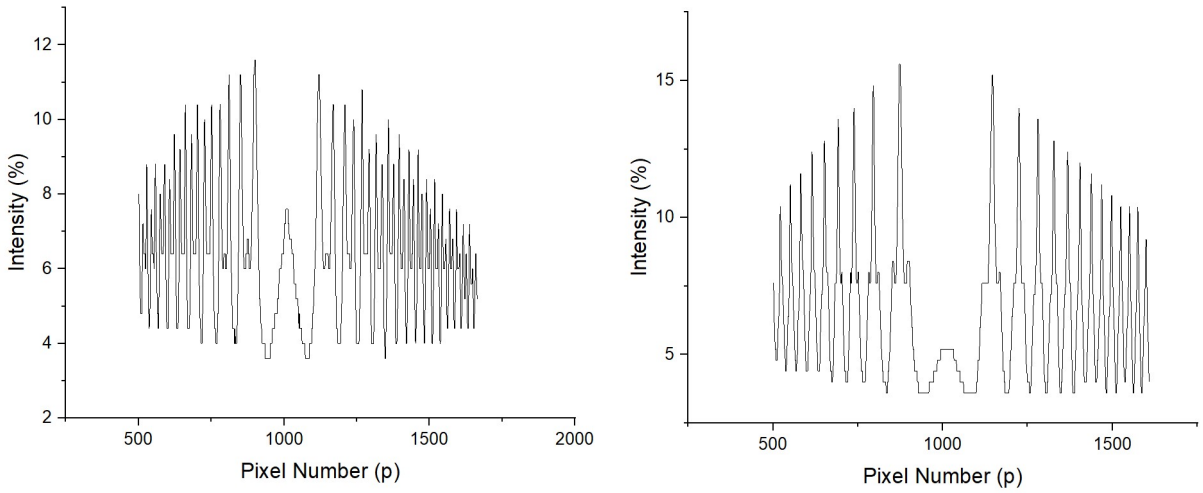

(a) Middle line of each triplet cancelled, quarter-wave plate (75°), linear polariser (15°).

(b) Outer lines of each triplet cancelled, quarter-wave plate (0°), linear polariser (90°).

Figure 5.5: Determination of polarisation states in the transverse normal Zeeman effect.

These plots show that when the linear polariser is set perpendicular to the magnetic field, only the light from the middle line of each triplet is transmitted. When the polarisers are set parallel to the magnetic field, only the light from the outer lines of each triplet is transmitted. This means that the light from all three transitions are linearly polarised where the centre line is polarised perpendicular to the magnetic field and the outer lines are polarised parallel to the magnetic field. This makes sense, since the central line is generated by dipole oscillations along the z-axis which is perpendicular to our optical axis, and the outer lines correspond to the rotation of dipoles in the x-y plane. In the transverse configuration, these rotations are basically viewed from an edge-on perspective and the resulting electromagnetic wave oscillates parallel to the magnetic field as it radiates.

3: Longitudinal Normal Zeeman Effect

After removing the polarisers and rotating the electromagnet by 90°, the interference maxima now appeared as doublets as shown below in Figure (5.6):

Figure 5.6: Doublet lines observed in the longitudinal configuration.

This proves that the radiation associated with a $\Delta M_J = 0$ transition is indeed produced by dipole oscillations along the direction of the magnetic field.

Once the eyepiece was replaced with the CCD and the analogous measurements of r and Δr were made for $I = (5, 6, 7)A$, the results were tabulated and are shown below.

Peak Radii and Shift of Radii for $I = 5A$					
m	r_m (pixels)	r_m (m)	Δr_m (m)	$r_m \Delta r_m$ (m^2)	$\delta r_m \Delta r_m$ (m^2)
1	115.45	1.62×10^{-3}	3.01×10^{-4}	4.87×10^{-7}	3×10^{-8}
2	202.1	2.83×10^{-3}	1.80×10^{-4}	5.08×10^{-7}	4×10^{-8}
3	259.9	3.64×10^{-3}	1.45×10^{-4}	5.29×10^{-7}	5×10^{-8}
4	306.9	4.30×10^{-3}	1.23×10^{-4}	5.30×10^{-7}	6×10^{-8}
5	347.5	4.86×10^{-3}	1.13×10^{-4}	5.48×10^{-7}	7×10^{-8}
6	384.1	5.38×10^{-3}	9.73×10^{-5}	5.23×10^{-7}	8×10^{-8}

Then for the next value of current:

Peak Radii and Shift of Radii for $I = 6A$					
m	r_m (pixels)	r_m (m)	Δr_m (m)	$r_m \Delta r_m$ (m^2)	$\delta r_m \Delta r_m$ (m^2)
1	116.1	1.63×10^{-3}	3.47×10^{-4}	5.65×10^{-7}	3×10^{-8}
2	202.9	2.84×10^{-3}	2.09×10^{-4}	5.92×10^{-7}	4×10^{-8}
3	260.1	3.65×10^{-3}	1.63×10^{-4}	5.97×10^{-7}	5×10^{-8}
4	307.5	4.31×10^{-3}	1.38×10^{-4}	5.96×10^{-7}	6×10^{-8}
5	348.25	4.88×10^{-3}	1.23×10^{-4}	6.01×10^{-7}	7×10^{-8}
6	384.6	5.38×10^{-3}	1.12×10^{-4}	6.01×10^{-7}	8×10^{-8}

Finally:

Peak Radii and Shift of Radii for $I = 7A$					
m	r_m (pixels)	r_m (m)	Δr_m (m)	$r_m \Delta r_m$ (m^2)	$\delta r_m \Delta r_m$ (m^2)
1	113.5	1.60×10^{-3}	3.76×10^{-4}	6.01×10^{-7}	3×10^{-8}
2	202	2.83×10^{-3}	2.16×10^{-4}	6.10×10^{-7}	4×10^{-8}
3	259.7	3.64×10^{-3}	1.69×10^{-4}	6.14×10^{-7}	5×10^{-8}
4	306.6	4.29×10^{-3}	1.51×10^{-4}	6.46×10^{-7}	6×10^{-8}
5	347.4	4.86×10^{-3}	1.32×10^{-4}	6.43×10^{-7}	7×10^{-8}
6	383.9	5.37×10^{-3}	1.18×10^{-4}	6.35×10^{-7}	8×10^{-8}

Using equation (3.3) the values of the shift $\Delta\lambda$ were then calculated and compared for the transverse and longitudinal configuration:

Comparison of $\Delta\lambda$: Longitudinal and Transverse				
I (A)	$\Delta\lambda$ (Transverse)	$\delta\Delta\lambda$ (Transverse)	$\Delta\lambda$ (Longitudinal)	$\delta\Delta\lambda$ (Longitudinal)
5	$6.39 \times 10^{-12} m$	$8 \times 10^{-13} m$	$7.02 \times 10^{-12} m$	$8 \times 10^{-13} m$
6	$7.40 \times 10^{-12} m$	$8 \times 10^{-13} m$	$7.98 \times 10^{-12} m$	$8 \times 10^{-13} m$
7	8.33×10^{-12}	$8 \times 10^{-13} m$	$8.42 \times 10^{-12} m$	$8 \times 10^{-13} m$

This shows that within experimental error, the shift of the wavelength caused by the external magnetic field only depends on the strength of the magnetic field and not the orientation. This agrees with the theoretical evaluation of the Zeeman effect which states that the sc scalar value of magnetic field strength is the factor responsible for the perturbation of the atomic energy spectrum.

The polarisation states were found for the longitudinal configuration in the same way as in section (2). The intensity graphs showing clear indication of the polarisation states of each line in the doublet are shown below in Figure (5.7):

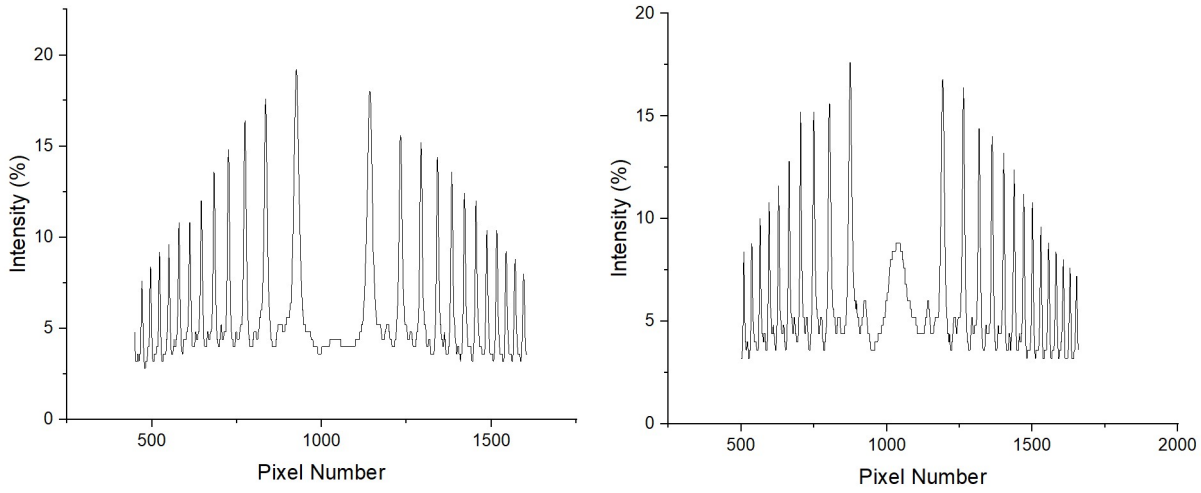

(a) Outer line of doublet cancelled, quarter-wave plate (45° anti-clockwise).

(b) Inner line of doublet cancelled, quarter-wave plate (45° clockwise).

Figure 5.7: Determination of polarisation states in the longitudinal normal Zeeman effect.

From these graphs we see that, in the longitudinal configuration, the light emitted by the neutral cadmium is circularly polarised for both lines in the doublet. With respect to this fact, the polarisation states could be found without use of the linear polariser. For the inner line, the polarisation is right-hand circular while for the outer line it is left-hand circular.

6 Conclusions

In this laboratory, we used a neutral Cadmium lamp to observe the normal Zeeman effect in both transverse and longitudinal orientations. The wavelength of the red cadmium line was found using an interference pattern generated by the Fabry Perot etalon. It was also observed that, in the presence of a magnetic field, the degeneracy of certain atomic energy levels could be removed and this resulted in the emission of a line doublet or triplet as opposed to a singlet in the corresponding emission spectrum. The value of the Bohr magneton was determined to be $\mu_B = 8.024 \times 10^{-24} \pm 0.5 \times 10^{-24}$ which varies from the value found in literature by approximately 15%, although this could be explained by prevailing experimental error. The red line of Cadmium was found to have a wavelength $\lambda = 639 \pm (20)nm$ which was significantly close to the known value. The polarisation states associated with the doublet and triplet lines were determined where the triplet seen in the transverse configuration consists of three linearly polarised waves and the doublet seen in the longitudinal configuration consists of two oppositely-circularly polarised waves. Overall the results of the experiment were satisfactory and agreed with the theoretical material.

7 Appendices

[1]:Zeeman P. "Verslagen van de Gewone Vergaderingen der Wis- en Natuurkundige Afdeeling" - [Reports of the Ordinary Sessions of the Mathematical and Physical Section (Royal Academy of Sciences in Amsterdam)], Vol. 5, pp.181-184, 242-248 (1896)

[2]: "An Introduction to Quantum Mechanics" - Griffiths (David. J.) (1982): 978-1-107-17986-8

[3]: Preston T. "Radiation Phenomena in the Magnetic Field". Nature 59 224 – 229 (1899)

[4]: "The Zeeman Effect" Lab Instruction Manual Trinity College Dublin School of Physics.

List of Figures